Nano-Sized Organo-Silica Particles with 'Built-In' SI-ATRP Capability as Platform for Brush Particle Synthesis

Jin Han[†,⊥,§], Yue Zhai[†,§], Zongyu Wang[‡,§], Markus Bleuel[‖♦], Tong Liu[‡], Rongguan Yin[‡], Wenjie Wu[°], Ilhem F. Hakem[#], Alamgir Karim[°], Krzysztof Matyjaszewski[*,‡], Michael R. Bockstaller[*,†]

[†]Department of Materials Science & Engineering, Carnegie Mellon University, 5000 Forbes Avenue, Pittsburgh, Pennsylvania 15213

[‡]Department of Chemistry, Carnegie Mellon University, 4400 Fifth Avenue, Pittsburgh, Pennsylvania 15213

[⊥]College of Materials Science and Engineering, Zhejiang University of Technology, Hangzhou, People's Republic of China 310014

[‖]NIST Center for Neutron Research, National Institute of Standards and Technology, Gaithersburg, MD 20988-8562

[♦]Department of Materials Science and Engineering, University of Maryland, College Park, MD 20742-2115

[°]Department of Chemical and Biomolecular Engineering, University of Houston, Houston, TX 77204

[#]Department of Chemical Engineering, Carnegie Mellon University, 5000 Forbes Avenue, Pittsburgh, Pennsylvania 15213

[§] J.H., Y.Z., and Z.W. contributed equally.

KEYWORDS: organosilica, particle, brush, SI-ATRP, SANS

ABSTRACT: A facile synthetic method was developed to prepare sub-5 nm organo-silica ($oSiO_2$) nanoparticles through the self-condensation of ATRP-initiator-containing silica precursors. The obtained $oSiO_2$ nanoparticles were characterized by a combination of nuclear magnetic resonance (NMR), thermogravimetric analysis (TGA), transmission electron microscopy (TEM), dynamic light scattering (DLS) and small-angle neutron scattering (SANS). The accessibility of the surface -Br initiating sites was evaluated by the polymerization of poly(methyl methacrylate) (PMMA) ligands from the surface of the $oSiO_2$ nanoparticles using surface-initiated atom transfer radical polymerization (SI-ATRP). The ultra-small size, tunable composition and ease of surface modification may render these organosilica nanoparticle systems with built-in SI-ATRP capability an interesting alternative to conventional silica nanoparticles for functional material design.

Over the past decades, silica nanoparticles have received much attention in diverse areas, such as catalysis, adsorption, separation and chromatography.[1-4] Due to the high level of biocompatibility and the well-established surface chemistry of silica that enables versatile functionalization of particle surfaces,[5] more recent applications of silica nanoparticles also include nanotechnology and nanomedicine. For example, silica nanoparticles have been utilized as biocompatible and multifunctional components in disease diagnosis and therapy and they have been widely explored as nanocarrier systems for drug delivery.[6-7] However, although small particle sizes are preferable in these applications, there are only few reports concerning the use of sub-10 nm particles,[8-10] as their synthesis has remained a challenge.[11-15] The chemical and thermal stability of nano-silica that derives from the high strength of Si-O bonds, has also fueled interest in the application of silica nanoparticles as platform for 'functional materials'. Examples are the synthesis of microporous templates with controlled morphology and porosity that have emerged as attractive host matrices for functional nanohybrids with applications ranging from catalysis to medicine or energy storage.[16-21]

Surface functionalization is of central importance for the application of silica nanoparticles and a variety of methods enabling the selective functionalization with multiple organic and inorganic groups have been demonstrated.[22] Especially, the modification of surfaces by polymer grafting techniques has become an important means for tailoring the surface of nanoparticles and the properties of the formed composite materials.[23-26] Controlled radical polymerization (CRP) procedures allow for the versatile synthesis of polymers with tunable molecular weight, narrow molecular weight distribution, and diverse architecture.[27] When applied to surface modification, CRP provides control of the composition, density, and length of surface-grafted polymer ligands.[28-30] However, often the required process involves multiple steps, i.e. the functionalization of initiator groups and subsequent surface polymerization. This can be detrimental to the viability of materials and thus limit their practical use.

In this contribution, we present a one-step process (based on the condensation of brominated organosilane precursors) to prepare initiator-modified organo-silica hybrid particles (C_y-$oSiO_2$-Br) with diameter of about 3 nm and narrow size dispersity. Here, 'Br' indicates the bromine functionalities that are intrinsic to the hybrid particles and

'C_y' indicates the composition (i.e. 'y' is the number of carbon atoms) of the vinyl alcohol used to synthesize the respective precursor (see below). The hybrid particles could readily be polymer-modified via surface-initiated atom transfer radical polymerization (SI-ATRP) without further surface modification.[24, 31]

The tetherable ATRP initiator, 3-(triethoxysilyl)alkyl α-bromoisobutyrate (TES-ABMP), was synthesized through the reaction between triethoxysilane (TES) and an intermediate, which was synthesized by reaction of vinyl alcohol derivatives (C_{x+2} $H_{2x+3}OH$) and α-bromoisobutyryl bromide (where 'x' corresponds to the number of methylene units and $y = x + 2$, Scheme S1). TES-ABMP could then be used to synthesize C_y-oSiO_2-Br hybrid nanoparticles with different sizes containing –Br groups, Scheme 1. The use of an initiator-containing precursor allowed skipping the functionalization steps before polymerization, thus avoiding the formation of extra atomic layers due to coupling reactions. In principle, this process allows for the variation of the number of initiating sites on the particles by changing the ratio between TES-ABMP and TES in the precursors. The particle size was found to be sensitive to the polarity of the solvent; in this work, organic solvent mixtures DMF: MeOH = 3:1 (vol/vol) were found to yield the most reproducible results, presumably due to the most favorable dissolution conditions of reactants.

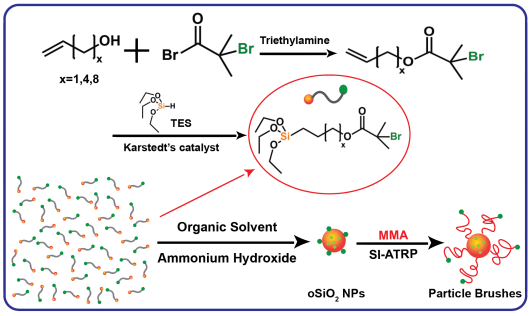

Scheme 1. Synthesis of oSiO_2 nanoparticles and oSiO_2-*g*-PMMA particle brushes.

In the following, the synthesis and characterization process will be illustrated for $x = 1$. The ^{1}H NMR (nuclear magnetic resonance) spectrum of the precursor is shown in Figure S1. The progress of the condensation reaction was studied by ^{29}Si NMR, as shown in Figure 1 which displays the results for the $x = 1$ precursor (3-(triethoxysilyl)propyl α-bromoisobutyrate, TES-PBMP). The signal of the silicon atom in the precursor silane appeared at -46.0 ppm as single sharp peak. The development of a much smaller peak at -47.0 ppm was ascribed to the silicon atom of minor amounts of hydrolyzed precursor silane (presumably caused by a small amount of water in the $CDCl_3$ solvent and the long time of the ^{29}Si NMR experiment). The silicon signal of the Si-O-Si moiety in the fully hydrolyzed and condensed C_3-oSiO_2-Br particles appeared at from (-65.0 to -71.0) ppm as a broad peak, which was in accordance with the -69.0 ppm signal of silicon in reference materials ($(c\text{-}C_6H_{11})_8Si_8O_{12}$) reported in the literature.[32]

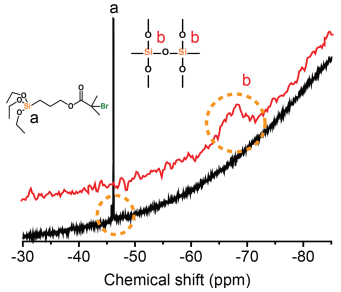

Figure 1. ^{29}Si NMR spectrum of the TES-PBMP precursor (black) and C_3-oSiO_2-Br hybrid nanoparticles (red).

Figure 2a shows the TEM images of the C_3-oSiO_2-Br nanoparticles which appeared well dispersed on the Cu grids without agglomeration. The average particle diameter was around 3 nm with narrow size distribution. This was in good agreement with the hydrodynamic diameter of 3.3±0.5 nm that was obtained by DLS (Fig. S2).

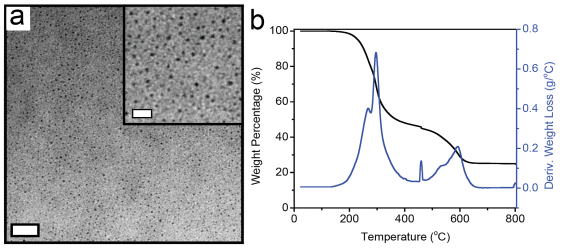

Figure 2. Characterization of structure and composition of C_3-oSiO_2-Br hybrid nanoparticles: (a) TEM image of C_3-oSiO_2-Br nanoparticles; scale bars: 50 nm, inset: 20 nm. (b) TGA curves of C_3-oSiO_2-Br nanoparticle product.

TGA analysis was performed to confirm the composition of the C_3-oSiO_2-Br nanoparticles, which is shown in Figure 2b. C_3-oSiO_2-Br nanoparticles displayed ~75 mass % of organic content. Moreover, two peaks are shown in the decomposition profile, one of which can be assigned to the weight loss between (250 and 300) °C and the other between (500 and 600) °C. The first transition shown in Figure 2b corresponds to approximately a 55% weight loss, suggesting that the thermal event was likely due to the removal of the bromoisobutyrate functional groups from the Si-O-Si framework (C_4H_6BrO). Assuming uniform crosslinking, the fraction of C_4H_6BrO (150 g/mol) is estimated to 57.7 mass % of the total molecular weight of C_3-oSiO_2-Br nanoparticles. The second transition, corresponding to approximately 20 mass %, confirms that this weight loss is caused by the removal of the alkyl fragments. The elemental analysis reveals that the molar mass of C_3H_6O is 58 g/mol, thus corresponding to about 22.3 mass % of the total mass of nanoparticles. The agreement between TGA results and elemental analysis supports that crosslinking during condensation was uniform. To evaluate the effect of precursor composition on the resulting size of hybrid particles, spacers with longer organic backbones x = 4, 8 (5-hexen-1-ol, 9-decen-1-ol) were employed using the same synthetic procedure (Scheme 1). Increasing x from 1 to 4 (C_6-oSiO_2-Br) resulted in the increase of organic content (79.8 % g/g) and particle size (4.2 nm, Figure S4).[15] Further increase to $x = 8$ (i.e. the 9-decen-1-ol system) did not result

in discrete nanoparticle products. Rather, small molecular clusters with a hydrodynamic diameter < 0.5 nm were observed. We attribute the observed effect of solvent polarity on particle size to be caused by the balance of increased organic content and decreased solubility with increasing x. For x = 1 and 4 reactants were found to be readily soluble. Thus, assuming equal degree of crosslinking, the increased organic content gives rise to increased particle size. In contrast, a reduced solubility was observed for x = 8, which constrained the crosslinking process.

To demonstrate and assess the activity of initiator groups that are presented at the surface, SI-ATRP was performed without prior surface modification. Scheme 1 illustrates the preparation process of C_3-oSiO_2-*g*-PMMA brush particles from the as-prepared C_3-oSiO_2-Br nanoparticles. The C_3-oSiO_2-*g*-PMMA particles brushes were synthesized by activators regenerated by electron transfer (ARGET) SI-ATRP. In the ARGET ATRP system, the amount of copper in the polymerization can be significantly reduced, since a fraction of the stable Cu^{II} complex is continuously reduced to the active Cu^{I}/L species by a reducing agent. Due to the complete condensation of the C_3-oSiO_2-Br precursor (Fig. 1), the product stock solution was directly used in the polymerization without purification thereby avoiding waste and agglomeration of the particles. Cu^{II} and highly active ligand Me_6TREN were chosen as the catalyst/ligand system. With 20 vol% initial monomer concentration, the reaction reached ~40 % conversion after 12 hours at 60 ºC, Table 1. The hybrid particle brushes were obtained by precipitation in cold MeOH for further characterization.

Table 1. Result of the synthesis of C_x-oSiO_2-Br nanoparticle and C_3-oSiO_2-*g*-PMMA particle brushes.

Entry[a]	x[b]	M_n[c]	M_w/M_n[c]	f_{SiO2}(%)[d]	f_{PMMA} (%)[e]	σ (nm^{-2})[f]	d_h(nm)[g]
C_3-oSiO_2-Br	1	N/A	N/A	24.87	N/A	N/A	3.3
C_6-oSiO_2-Br	4	N/A	N/A	20.19	N/A	N/A	4.2
C_{10}-oSiO_2-Br	8	N/A	N/A	-	N/A	N/A	0.4
Entry[a]	D:H molar ratio	M_n[c]	M_w/M_n[c]	f_{SiO2} (%)[d]	f_{PMMA} (%)[e]	σ (nm^{-2})[f]	*SLD* (10^{-6} Å^{-2})[h]
C_3-oSiO_2-*g*-PMMA	0:100	17,550	1.39	4.56	81.66	0.122	1.05
C_3-oSiO_2-*g*-10%dPMMA	10:90	17,930	1.44	3.97	84.03	0.140	1.63
C_3-oSiO_2-*g*-20%dPMMA	20:80	18,300	1.49	4.03	83.80	0.136	2.22
C_3-oSiO_2-*g*-30%dPMMA	30:70	18,590	1.38	3.38	86.41	0.165	2.80
C_3-oSiO_2-*g*-40%dPMMA	40:60	16,910	1.34	3.94	84.16	0.151	3.38
C_3-oSiO_2-*g*-50%dPMMA	50:50	18,060	1.42	2.83	88.62	0.208	3.97

[a] Reaction condition:$[MMA]_0/[C_3\text{-o}SiO_2]_0/[CuBr_2]_0/[Me_6TREN]_0:[Sn(EH)_2]_0$ = 400:1:0.5:5:2, with 30 vol% anisole, 33 vol% DMF, 17 vol% methanol, at 60 ºC, $[MMA]_0$ = 1.8 M, reaction time is 12 h. [b] Number of spacer (carbon atom) in nanoparticle precursors. [c] Determined by SEC. [d] Mass fraction (% g/g) of silica content determined by TGA. [e] Calculated from Eq. S1 according to TGA data. [f] Calculated from Eq. S2 according to TGA data. [g] Hydrodynamic size of C_3-oSiO_2-Br nanoparticle and particle brushes determined by DLS. [h] Scattering length density of PMMA polymer brushes which is calculated from equation S3.

The molecular weight of PMMA ligands, was determined after etching of C_3-oSiO_2-*g*-PMMA to be M_n = 17,550 with dispersity M_w/M_n = 1.39. Concurrent with polymer modification, a significant increase of the hydrodynamic diameter from (3.3 to 11) nm was observed. Electron micrographs such as shown in Figure 3a revealed uniform particle morphologies as well as an increase on the particle surface-to-surface distance. The core size of C_3-oSiO_2 remained about constant during the polymerization. Figure 3b shows the TGA curves of C_3-oSiO_2-Br nanoparticle and the corresponding particle brush product. The mass fraction of PMMA polymer in the C_3-oSiO_2-*g*-PMMA system was determined after normalization (Eq. S1) to be 81.7 % g/g. Brush particles could be processed (by solvent casting) to form mechanically robust and transparent films (Fig. 3c). Note that due to the small size of the nanoparticles and the

uniform microstructure of the brush particle hybrids, the scattering loss of the particle fillers was negligible, and the bulk film exhibited outstanding transparency at thickness around 500 μm (Fig. 3c).

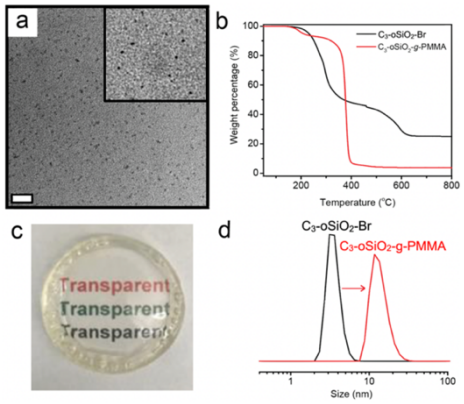

Figure 3. Characterization of C_3-oSiO$_2$-*g*-PMMA hybrid particles. (a) TEM image of C_3-oSiO$_2$-*g*-PMMA particle brush, scale bars: 50 nm; inset scale bar: 20 nm; (b) TGA curves of C_3-oSiO$_2$-Br nanoparticles (black) and C_3-oSiO$_2$-*g*-PMMA particle brushes (red); (c) photograph of C_3-oSiO$_2$-*g*-PMMA bulk film , film size is 1.2 inches (diameter) by 0.5 mm (thickness); (d) DLS number distribution of C_3-oSiO$_2$-Br nanoparticles (black) and C_3-oSiO$_2$-*g*-PMMA particle brushes (red).

To further elucidate the structure and composition of C_3-oSiO$_2$-Br and C_3-oSiO$_2$-*g*-PMMA hybrid particles, small-angle neutron scattering (SANS) on partially deuterated homologs was performed. The specific objective of neutron scattering experiments was to infer the approximate elemental composition of organosilica cores by determination of the 'minimum contrast' condition of films formed by brush particles tethered with selectively deuterated PMMA. The total scattering of films was measured in terms of the scattering invariant Q_{inv} which was determined from the scattering intensity via $Q_{inv} = 4\pi \int I(q)q^2 dq$ where q is the momentum of the scattering vector and $I(q)$ is the (background-corrected) scattered intensity.[33] The scattering invariant for a two-phase system is given as $Q_{inv} = 2\pi^2\phi(1-\phi)(\Delta SLD)^2$, where ϕ is the volume fraction and ΔSLD is the scattering length density contrast between the phases.[34] Thus, the invariant would vanish if the scattering length density of polymer ligands and core are matched (i.e. $SLD_{PMMA} = SLD_{core}$). Conversely, if Q_{inv} vanishes and the SLD_{PMMA} of polymer tethers is known, then SLD_{core} can be determined. Since the scattering length density of a material depends on its elemental composition (see Eq. 3 in Supporting Information), this process could be used to independently validate the composition of C_3-oSiO$_2$-*g*-PMMA particles.[35] A series of hybrid particle analogs with about equal composition but systematically varied degree of deuteration of PMMA tethers was synthesized by using appropriate mixtures of hydrogenated and deuterated (d8) MMA monomers (see Table 1). Since deuteration is not expected to affect the polymerization kinetics, the final deuteration fraction of partially deuterated brush particles was assumed to be equal to the monomer H/D molar ratio.

The scattering length density of the polymer brush could be calculated from Eq. S3 and is summarized in Table 1. These six samples were solvent-casted in a Teflon mold to form free-standing films with thickness of 500 µm. Small angle neutron scattering was performed using NGB 30m SANS instrument at NIST.

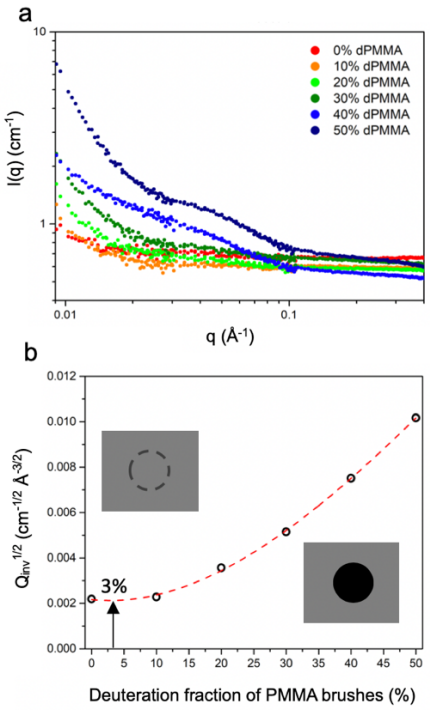

Figure 4. a) Scattered intensity profile $I(q)$ for C_3-oSiO$_2$-*g*-(d/h) PMMA particle brush films with error bar representing one sigma uncertainties. The upwards trend of $I(q)$ in the limit of small q is attributed to film inhomogeneities. b) Scattering invariant determined by integration of the scattering intensity between (0.028 and 0.11) Å^{-1}. The minimum point is found at approximately 3% deuteration.

Figure 4a shows the corresponding 1D scattered intensity curves of all systems after correction for empty beam and blocked beam. The invariant was determined by integration of the respective $I(q)$ data (corrected for incoherent scattering) and is displayed in Figure 4b. A cubic polynomial was fitted to the invariant data to determine the deuteration fraction corresponding to the minimum scattering invariant as $f_D = 0.03$. This corresponds to scattering length density of polymer tethers (and core) of 1.23 10^{-6} Å^{-2}. From this result the mass density of organosilica nanoparticles was determined using Eq. S4 to be 1.61 g/cm^3. Moreover, based on the molar mass, density and size of a single particle from SANS, DLS and TEM, an average number of 71 siloxane repeat units per particle core was calculated. According to Eq. S2, the grafting density of C_3-oSiO$_2$-g-PMMA brush particles is 0.12 chains/nm^2, corresponding to an average of 5 chains per particle. Therefore, the apparent Br initiation efficiency was estimated to be about 7%. This suggests that a significant fraction of Br atoms was 'buried' within the particle and thus not accessible to the grafting-from process. Thus, the technique described herein might be most useful

for the synthesis of brush particle systems with intermediate grafting densities.[36]

In conclusion, a method for the synthesis of sub-5 nm initiator-modified organo-SiO_2 nanoparticles through the condensation of ATRP-initiator-containing silica precursor was developed. One-step grafting-from polymerization (without the need of purification or surface modification) using ARGET SI-ATRP resulted in brush particle products with grafting densities > 0.1 nm^{-2}. Si-NMR in conjunction with SANS analysis demonstrated near complete crosslinking of precursor species. Organo-silica nanoparticles exhibited up to 75 mass % organic content resulting in a mass density of 1.61 g/cm^3. We expect that the method provides a versatile platform for the synthesis of functional nano-silica materials with application in areas like sensing, medical therapy, drug delivery, and energy storage field. For example, additional functionalities could be introduced by using appropriately composed precursor blends. Future research will establish the robustness of the method to changes in precursor composition or process conditions.

ASSOCIATED CONTENT

Supporting Information. Synthetic procedures, NMR, DLS, and TGA characterization data. The Supporting Information is available free of charge on the (…) Publications website at (…).

AUTHOR INFORMATION

Corresponding Author

* E-mail: km3b@andrew.cmu.edu (K.M.)

* E-mail: bockstaller@cmu.edu (M.R.B.)

Author Contributions

J.H., Y.Z and Z.W. synthesized materials and performed characterization work. T.L., M.B., R.Y and W.W assisted in the synthesis and characterization work. I.F.H. and A.K. assisted in the interpretation of data. K.M. and M.B. conceived and organized the project. J.H., Y.Z. and Z.W. contributed equally.

Notes

The authors declare no competing financial interest.

ACKNOWLEDGMENT

This work was supported by the Department of Energy (DE-SC0018784). Access to USANS BT5 and NGB30SANS was provided by the Center for High Resolution Neutron Scattering, a partnership between the National Institute of Standards and Technology and the National Science Foundation under Agreement DMR-1508249. The authors acknowledge use of the Materials Characterization Facilities at Carnegie Mellon University supported by Grant MCF-678085 (electron imaging) and Cedric Gagnon for help with the SANS setup.

Disclaimer

Specific commercial equipment, instruments, or materials are identified in this paper to foster understanding. Such identification does not imply recommendation or endorsement by the National Institute of Standards and Technology, nor does it imply that the materials or equipment identified are necessarily the best available for the purpose.

REFERENCES

(1) Huo, Q.; Leon, R.; Petroff, P. M.; Stucky, G. D., Mesostructure Design with Gemini Surfactants: Supercage Formation in a Three-Dimensional Hexagonal Array. *Science* **1995,** *268* (5215), 1324-1327.

(2) Bagshaw, S. A.; Prouzet, E.; Pinnavaia, T. J., Templating of Mesoporous Molecular Sieves by Nonionic Polyethylene Oxide Surfactants. *Science* **1995,** *269* (5228), 1242-1244.

(3) Areva, S.; Boissière, C.; Grosso, D.; Asakawa, T.; Sanchez, C.; Lindén, M., One-pot aerosol synthesis of ordered hierarchical mesoporous core–shell silica nanoparticles. *Chem. Commun.* **2004,** (14), 1630-1631.

(4) Tarn, D.; Ashley, C. E.; Xue, M.; Carnes, E. C.; Zink, J. I.; Brinker, C. J., Mesoporous Silica Nanoparticle Nanocarriers: Biofunctionality and Biocompatibility. *Acc. Chem. Res.* **2013,** *46* (3), 792-801.

(5) Rossi, L. M.; Shi, L.; Quina, F. H.; Rosenzweig, Z., Stöber Synthesis of Monodispersed Luminescent Silica Nanoparticles for Bioanalytical Assays. *Langmuir* **2005,** *21* (10), 4277-4280.

(6) Vallet-Regi, M.; Rámila, A.; del Real, R. P.; Pérez-Pariente, J., A New Property of MCM-41: Drug Delivery System. *Chemistry of Materials* **2001,** *13* (2), 308-311.

(7) Ow, H.; Larson, D. R.; Srivastava, M.; Baird, B. A.; Webb, W. W.; Wiesner, U., Bright and Stable Core−Shell Fluorescent Silica Nanoparticles. *Nano Lett.* **2005,** *5* (1), 113-117.

(8) Fowler, C. E.; Khushalani, D.; Lebeau, B.; Mann, S., Nanoscale Materials with Mesostructured Interiors. *Advanced Materials* **2001,** *13* (9), 649-652.

(9) Büchel, G.; Grün, M.; Unger, K. K.; Matsumoto, A.; Kazuo, T., Tailored syntheses of nanostructured silicas: Control of particle morphology, particle size and pore size. *Supramolecular Science* **1998,** *5* (3), 253-259.

(10) Suzuki, K.; Ikari, K.; Imai, H., Synthesis of Silica Nanoparticles Having a Well-Ordered Mesostructure Using a Double Surfactant System. *Journal of the American Chemical Society* **2004,** *126* (2), 462-463.

(11) Ma, K.; Sai, H.; Wiesner, U., Ultrasmall Sub-10 nm Near-Infrared Fluorescent Mesoporous Silica Nanoparticles. *Journal of the American Chemical Society* **2012,** *134* (32), 13180-13183.

(12) Quan, B.; Lee, C.; Yoo, J. S.; Piao, Y., Facile scalable synthesis of highly monodisperse small silica nanoparticles using alkaline buffer solution and their application for efficient sentinel lymph node mapping. *Journal of Materials Chemistry B* **2017,** *5* (3), 586-594.

(13) Yokoi, T.; Wakabayashi, J.; Otsuka, Y.; Fan, W.; Iwama, M.; Watanabe, R.; Aramaki, K.; Shimojima, A.; Tatsumi, T.; Okubo, T., Mechanism of Formation of Uniform-Sized Silica Nanospheres Catalyzed by Basic Amino Acids. *Chemistry of Materials* **2009,** *21* (15), 3719-3729.

(14) Tran, V.-L.; Thakare, V.; Rossetti, F.; Baudouin, A.; Ramniceanu, G.; Doan, B.-T.; Mignet, N.; Comby-Zerbino, C.; Antoine, R.; Dugourd, P.; Boschetti, F.; Denat, F.; Louis, C.; Roux, S.; Doussineau, T.; Tillement, O.; Lux, F., One-pot direct synthesis for multifunctional ultrasmall hybrid silica nanoparticles. *Journal of Materials Chemistry B* **2018,** *6* (29), 4821-4834.
(15) Zhang, J.; Song, Y.; Zhao, Y.; Zhao, S.; Yan, J.; Lee, J.; Wang, Z.; Liu, S.; Yuan, R.; Luo, D.; Kopeć, M.; Gottlieb, E.; Kowalewski, T.; Matyjaszewski, K.; Bockstaller, M. R., Organosilica with Grafted Polyacrylonitrile Brushes for High Surface Area Nitrogen-Enriched Nanoporous Carbons. *Chem. Mater.* **2018,** *30* (7), 2208-2212.
(16) Lin, Y.-S.; Haynes, C. L., Synthesis and Characterization of Biocompatible and Size-Tunable Multifunctional Porous Silica Nanoparticles. *Chemistry of Materials* **2009,** *21* (17), 3979-3986.
(17) Wang, L.; Bai, J.; Li, Y.; Huang, Y., Multifunctional Nanoparticles Displaying Magnetization and Near-IR Absorption. *Angewandte Chemie International Edition* **2008,** *47* (13), 2439-2442.
(18) Kim, J.; Lee, J. E.; Lee, S. H.; Yu, J. H.; Lee, J. H.; Park, T. G.; Hyeon, T., Designed Fabrication of a Multifunctional Polymer Nanomedical Platform for Simultaneous Cancer- Targeted Imaging and Magnetically Guided Drug Delivery. *Advanced Materials* **2008,** *20* (3), 478-483.
(19) Feng, C.; Pang, X.; He, Y.; Li, B.; Lin, Z., Robust Route to Unimolecular Core–Shell and Hollow Polymer Nanoparticles. *Chem. Mater.* **2014,** *26* (20), 6058-6067.
(20) Feng, C.; Pang, X.; He, Y.; Chen, Y.; Zhang, G.; Lin, Z., A versatile strategy for uniform hybrid nanoparticles and nanocapsules. *Polym. Chem.* **2015,** *6* (29), 5190-5197.
(21) He, Y.; Yoon, Y. J.; Harn, Y. W.; Biesold-McGee, G. V.; Liang, S.; Lin, C. H.; Tsukruk, V. V.; Thadhani, N.; Kang, Z.; Lin, Z., Unconventional route to dual-shelled organolead halide perovskite nanocrystals with controlled dimensions, surface chemistry, and stabilities. *Science Advances* **2019,** *5* (11), eaax4424.
(22) Trewyn, B. G.; Slowing, I. I.; Giri, S.; Chen, H.-T.; Lin, V. S. Y., Synthesis and Functionalization of a Mesoporous Silica Nanoparticle Based on the Sol–Gel Process and Applications in Controlled Release. *Accounts of Chemical Research* **2007,** *40* (9), 846-853.
(23) Li, C.; Benicewicz, B. C., Synthesis of Well-Defined Polymer Brushes Grafted onto Silica Nanoparticles via Surface Reversible Addition−Fragmentation Chain Transfer Polymerization. *Macromolecules* **2005,** *38* (14), 5929-5936.
(24) Hui, C. M.; Pietrasik, J.; Schmitt, M.; Mahoney, C.; Choi, J.; Bockstaller, M. R.; Matyjaszewski, K., Surface-Initiated Polymerization as an Enabling Tool for Multifunctional (Nano-)Engineered Hybrid Materials. *Chem. Mater.* **2014,** *26* (1), 745-762.
(25) Tsujii, Y.; Ohno, K.; Yamamoto, S.; Goto, A.; Fukuda, T., Structure and Properties of High-Density Polymer Brushes Prepared by Surface-InitiatedLiving Radical Polymerization. In *Surface-Initiated Polymerization I*, Jordan, R., Ed. Springer Berlin Heidelberg: Berlin, Heidelberg, **2006**, pp 1-45.
(26) Yan, J.; Bockstaller, M. R.; Matyjaszewski, K., Brush-modified materials: Control of molecular architecture, assembly behavior, properties and applications. *Prog. Polym. Sci.* **2020,** *100*, 101180.
(27) Matyjaszewski, K.; Xia, J., Atom Transfer Radical Polymerization. *Chemical Reviews* **2001,** *101* (9), 2921-2990.
(28) Prucker, O.; Rühe, J., Synthesis of poly(styrene) monolayers attached to high surface area silica gels through self-assembled monolayers of azo initiators. *Macromolecules* **1998,** *31* (3), 592-601.
(29) Matyjaszewski, K., Advanced Materials by Atom Transfer Radical Polymerization. *Adv. Mater.* **2018,** *30* (23), 1706441.
(30) Matyjaszewski, K., Atom Transfer Radical Polymerization (ATRP): Current Status and Future Perspectives. *Macromolecules* **2012,** *45* (10), 4015-4039.
(31) Matyjaszewski, K.; Miller, P. J.; Shukla, N.; Immaraporn, B.; Gelman, A.; Luokala, B. B.; Siclovan, T. M.; Kickelbick, G.; Vallant, T.; Hoffmann, H.; Pakula, T., Polymers at Interfaces: Using Atom Transfer Radical Polymerization in the Controlled Growth of Homopolymers and Block Copolymers from Silicon Surfaces in the Absence of Untethered Sacrificial Initiator. *Macromolecules* **1999,** *32* (26), 8716-8724.
(32) Pescarmona, P. P.; Maschmeyer, T., Review: Oligomeric Silsesquioxanes: Synthesis, Characterization and Selected Applications. *Aust. J. Chem.* **2002,** *54* (10), 583-596.
(33) Glinka, C. J.; Barker, J. G.; Hammouda, B.; Krueger, S.; Moyer, J. J.; Orts, W. J., The 30 m Small-Angle Neutron Scattering Instruments at the National Institute of Standards and Technology. *J. Appl. Crystallogr.* **1998,** *31* (3), 430-445.
(34) Roe, R. In *Methods of X-ray and neutron scattering in polymer science*, **2000**.
(35) Sears, V. F. In *Neutron scattering lengths and cross sections*, **1992**.
(36) Lee, J.; Wang, Z.; Zhang, J.; Yan, J.; Deng, T.; Zhao, Y.; Matyjaszewski, K.; Bockstaller, M. R., Molecular Parameters Governing the Elastic Properties of Brush Particle Films. *Macromolecules* **2020,** *53* (4), 1502-1513.

TOC Graphics

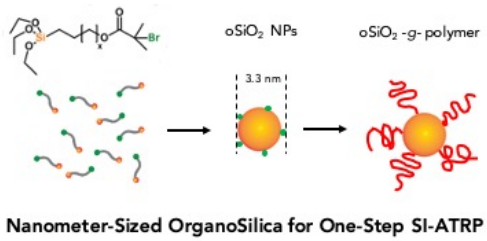

Nanometer-Sized OrganoSilica for One-Step SI-ATRP